Microstructural evolution of 3YSZ flash-sintered with current ramp control

Isabela R. Lavagnini[1]*; João V. Campos[1]; Julieta A. Ferreira[1]; Eliria M. J. A. Pallone[1].
[1]Departamento de Engenharia de Biossistemas, Universidade de São Paulo, USP
Av. Duque de Caxias Norte, 225, Pirassununga-SP, Brasil.

Abstract

The effect of a controlled current ramp (CR) during flash sintering on the densification and microstructural evolution of zirconia stabilized with 3 mol% yttria (3YSZ) was investigated. To this end, samples were flash-sintered with CR control at six electric current density ramp rates and compared with samples flash-sintered without a CR. Electric current density of 100 and 200 $mA{\cdot}mm^{-2}$ were used. The microstructure of cylindrical samples flash-sintered with and without a CR were observed. Grain size heterogeneity between the curved surface and the core was observed in all flash-sintered samples regardless of the electric current density used. By contrast, the samples sintered under a CR exhibited a homogeneous grain size, especially when the electric current density was 100 $mA{\cdot}mm^{-2}$.

Keywords: Field Assisted Sintering Technology (FAST), microstructure, zirconia: yttria stabilized, zirconia, current ramp control.

Introduction

Flash sintering (FS) was first reported by Cologna et al.[1] This technique allows the sintering of different materials under temperatures hundreds of degrees lower than those used in conventional sintering. In addition, it can reduce the processing time from hours to seconds compared to conventional sintering.[1–5]

The electrical parameters of the FS technique, e.g., the electric field and electric current density, can significantly affect the characteristics of the sintered material.[5–11] At certain values of these parameters, the grain size distribution in the sample may be heterogeneous.[10,12–14]

Steil et al.[12] observed microstructural heterogeneity between the center and the surface of zirconia stabilized with 8 mol% yttria (8YSZ) flash-sintered under relatively severe electric field and current conditions. This heterogeneity may be attributable to the heat transfer mechanisms in the sample during FS. At high temperatures, heat is expected to dissipate more quickly by radiation at the surface than at the center of the sample. Consequently, a temperature gradient is formed between the core and the surface. Thus, grains in the core of the sample are expected to be larger than those on the surface.[15,16]

The presence of hotspots during FS may also cause grain size heterogeneity. When conditions favor electric current passage in some regions of the sample, hotspots can occur, resulting in localized enhancement of grain growth.[14] In general, hotspots occur in samples with large volumes or under high electric field and electric current values.[17,18] Considering that pores in the green bodies may also affect the preferred current path, the green density and conformation method may also be related to hotspot formation.[13]

Ren et al.[19] flash-sintered zirconia stabilized with 3 mol% yttria (3YSZ) using a DC electric field. They observed grains with different sizes in the regions near the anode and the cathode. This heterogeneity can occur because of the observed thermal differences between these two regions.[20] In a work on 8YSZ monocrystals, Biesuz et al.[20] suggested that this temperature gradient may be related to partial electrochemical reduction, which is also called blackening.[21] They observed that blackening starts in the region of the sample in contact with the cathode and then spreads through the sample until it reaches the anode side, which results in an electrical conductivity gradient between the cathode and anode. Thus, regions with lower electrical conductivity should exhibit higher Joule heating, and thus higher temperature. As the cathode has higher electrical conductivity, its temperature is lower than that of the anode.[20] Campos et al.[10] suggested that this temperature difference could be responsible for the grain size difference in 3YSZ flash-sintered in a DC electric field.

Du et al.[22] and Campos et al.[10] observed heterogeneous microstructure in cylindrical samples of 8YSZ and 3YSZ, respectively, obtained by FS under an AC electric field. A grain size difference was found between the surfaces in contact with the electrode (the flat surfaces) and the core of the sample. This difference can be attributed to the lower temperature near the electrodes compared to that at the core of the samples during sintering under an AC electric field.[20] According to Liu et al.[23], the region near the electrodes may be cooler than the core because of the endothermic nature of the reduction and oxidation reactions occurring at the cathode and anode. In addition, platinum electrodes have higher thermal conductivity than air; thus, the electrodes can act as heat sinks.[10]

The properties of materials are related to their microstructure; therefore, knowledge of the grain growth kinetics associated with different FS parameters is essential. Thus, one challenge of FS is the production of ceramics with homogeneous microstructure.[24] Some authors believe that it may be possible to avoid heterogeneous microstructure in flash-sintered materials by gradually increasing the electric current using a current ramp (CR). The abrupt increase in the current observed in conventional FS may be related to the thermal gradient in the samples during the flash phenomenon and cause the grain size heterogeneity between the core and surface.[10,25]

The use of a CR in sintering of 3YSZ has resulted in microstructural homogeneity in experiments using a DC electric field (dog-bone-shaped samples)[15] and an AC electric field (cylindrical samples)[10]. Other studies have shown that a CR increased the densification of zinc oxide samples compared with that obtained by FS without a CR.[24,26]

Therefore, the present work evaluates the effect of the electric current density ramp rate under an AC electric field during the flash phenomenon on the homogeneity of the microstructure of 3YSZ.

Material and methods

Samples were prepared using a commercial 3YSZ powder (TZ-3Y-E, Tosoh). The average particle size of the powder was 40 nm, and the theoretical density (TD) was 6.05 $g{\cdot}cm^{-3}$. A mixture of the commercial 3YSZ powder, 0.5% 4-aminobenzoic acid (Vetec LTDA) by mass, and 0.5% oleic acid (Vetec LTDA) by mass was mixed in alcohol using a ball mill for 22 h. The resulting suspension was dried under continuous air flow at room temperature.[27] The samples were uniaxially pressed into cylinders 6 mm in diameter and 5 mm in height and then isostatically pressed at 200 MPa.

Then, the samples were calcined at 800 °C for 1 h with a heating rate of 5 °C·min^{-1}.

Sintering was performed in an automated tubular furnace adapted for sintering under an electric field.[10] A heating rate of 20 °C·min^{-1} was used under an applied sinusoidal electric field of 120 V·cm^{-1} (RMS) and a frequency of 1000 Hz. Platinum electrodes were placed on the flat top and bottom surfaces of the sample. Platinum wires were used to connect the electrodes to a power supply (PS) (751iX, California Instruments). No conductive paste was used. However, a uniaxial mechanical pressure of 3 bar was applied to maintain contact between the sample and the electrodes. A linear variable differential transformer was used as a displacement sensor to record the specific linear shrinkage *in situ* during sintering.

In the CR experiments, the AC electric field was applied to the sample from the beginning of furnace heating (voltage-to-current experiments). The PS was programmed to control the voltage until the electric current density reached 10 mA·mm^{-2}. Next, the PS switched from voltage control to electric current control. Then automatic control of the CR at various ramp rates was initiated. In each experiment, one of six different ramps was implemented until an electric current density of 100 or 200 mA·mm^{-2} (RMS) was reached. Then, the PS was turned off. For comparison, FS without a controlled CR was performed using the same electrical parameters. In this case, the PS remained on for 142 s after the electric current density reached 100 mA·mm^{-2} and for 300 s after it reached 200 mA·mm^{-2}. This time was calculated to provide the same energy as that supplied by the PS to the CR samples at the lowest ramp rates. Experiments were conducted in triplicate under each condition. Table 1

summarizes the conditions under which the CR and FS experiments were performed.

Table 1. FS and CR conditions.

Sample	Maximum current density ($mA \cdot mm^{-2}$)	Ramp rate ($mA \cdot mm^{-2} \cdot s^{-1}$)
1FS	100	-
1CR100		1.64
2CR100		0.82
3CR100		0.41
2FS	200	-
1CR200		5.66
2CR200		1.89
3CR200		0.63

The apparent densities of the samples were determined using the Archimedes principle according to ASTM C373-88[28]; the averages were expressed as a function of the TD (% TD).

The microstructure at the radial centers of the cross-sectional polished surfaces was analyzed using scanning electron microscopy (SEM, FEG-XL 30, Philips). To analyze the microstructure obtained under different sintering conditions, micrographs were obtained in different regions of the sample, specifically, the core and the curved surface at the half-height of the cylindrical samples. Figure 1 shows the regions where the micrographs were obtained.

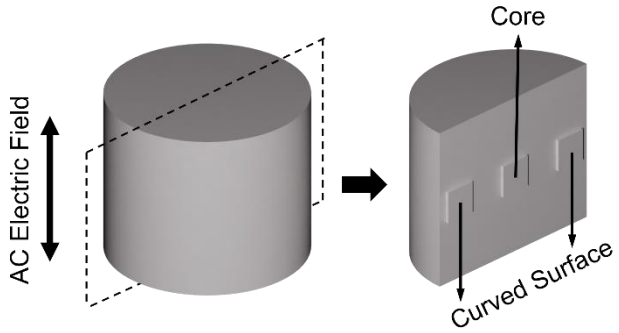

Figure 1. a) Radial longitudinal section of a cylindrical sample and b) its polished surface, focusing on the regions in which the microstructure was analyzed.

The grain size in each region was calculated using ImageJ software (public domain, developed by the National Institutes of Health, US). The average grain size in each region of the same sample were evaluated by analysis of variance using the Tukey test, with a significance level of 5%.

Results and discussion

Figure 2 shows the electric current density, electric field, and electric power density curves of samples 1FS, 2FS, 3CR100, and 3CR200. The behavior of the curves demonstrates the differences between FS and CR. At the beginning of both the FS and CR techniques, the PS was in voltage control mode at 120 $V \cdot cm^{-1}$.

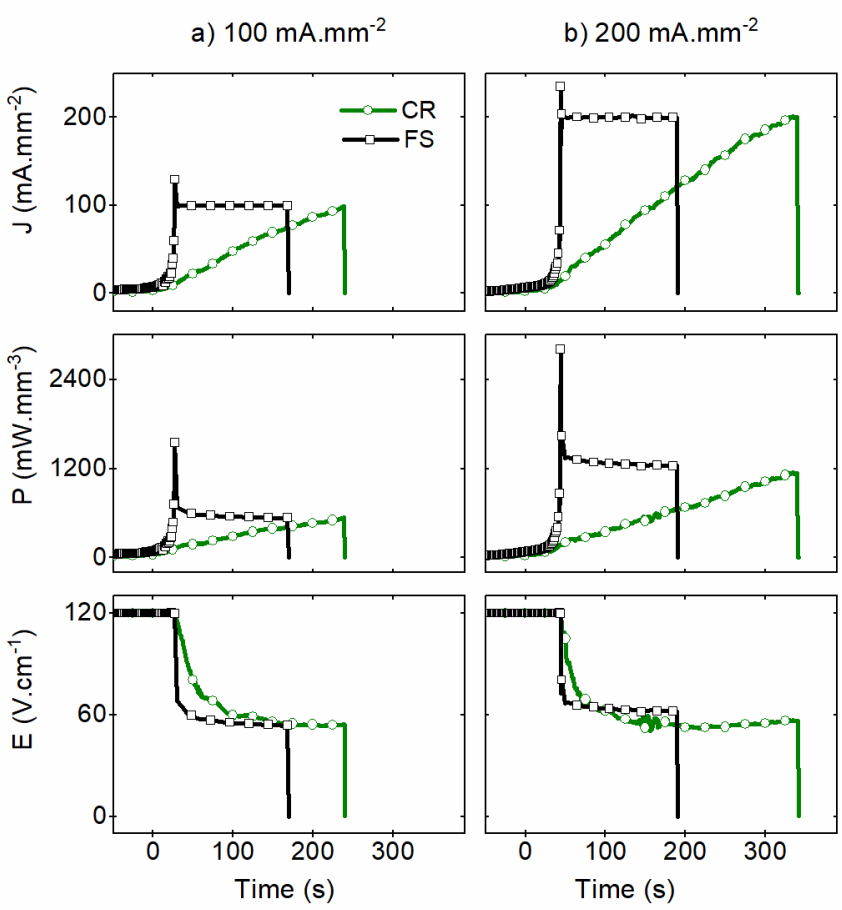

Figure 2. Plots of electric current density (J), electric power density (P), and electric field (E) as a function of time for samples 1FS, 2FS, 3CR100, and 3CR200.

When the CR was applied, the PS was changed from voltage control mode to electric current control mode when a density of 10 $mA \cdot mm^{-2}$ was reached. In contrast, when FS was performed, the PS was switched to electric current control mode only when the current density reached the maximum predetermined value (100 or 200 $mA \cdot mm^{-2}$). Then, the electric field decreased owing to the increased electrical conductivity of the samples due to thermal runaway, which indicated the flash onset.[29]

The final electric fields of the flash sintered and CR samples treated at 100 and 200 $mA \cdot mm^{-2}$ were approximately 54 and 60 $V \cdot cm^{-1}$,

respectively. According to Ohm's law, higher electric field values are expected for samples under a current density of 200 $mA{\cdot}mm^{-2}$. Thus, after densification of samples with similar electrical conductivity, a higher electric field is expected to maintain a higher electric current through the samples.

In all conditions studied the furnace temperature at the time of the flash event was between 990 and 1000 °C, but the sample temperature increases in proportion to the electric power density applied by the PS. The power density curves (Figure 2) indicate a relationship between the sample's temperature and the applied power. However, during FS, the power density increases abruptly and in an uncontrolled way, making it difficult to determine the maximum temperature reached by the sample.[6] In addition, power peaks were observed for the flash sintered samples (Figure 2) at the moment the PS switched to electric current control mode. For the 1FS and 2FS samples, the power reached approximately 1549 and 2809 $mW{\cdot}mm^{-3}$, respectively, at these peaks. When the voltage control switched to electric current control, an internal capacitor in the PS discharged, generating power peaks in the FS experiments. This behavior significantly increased the electric power applied to the sample in a short period of time, and the pre-established values of the electric current may have been momentarily exceeded.[7,12,30]

Note that the CR samples did not show any power peak, and the highest values were 540 and 1136 $mW{\cdot}mm^{-3}$ for the samples treated at 100 and 200 $mA{\cdot}mm^{-2}$, respectively. These values are much lower than those of the flash sintered samples. The power density curves of the CR samples were similar to the electric current density curves (Figure 2). As discussed earlier, for the PS to provide the same amount of energy to the FS and CR samples, the integrals of the analytical curve of the electric

power density (which represents the energy supplied by the PS) have equal values (90.7 J·mm^{-3} for samples 1FS and 3CR100 and 197.0 J·mm^{-3} for samples 2FS and 3CR200).

Figure 3 shows the linear shrinkage curves as a function of time for the FS and CR samples treated at 100 and 200 mA·mm^{-2}. As expected, most of the linear shrinkage of the samples in the FS experiments occurred abruptly as the electric current density increased. By contrast, in the CR samples, the linear shrinkage increased gradually. The rate of linear shrinkage generally decreased with decreasing electric current ramp rate.

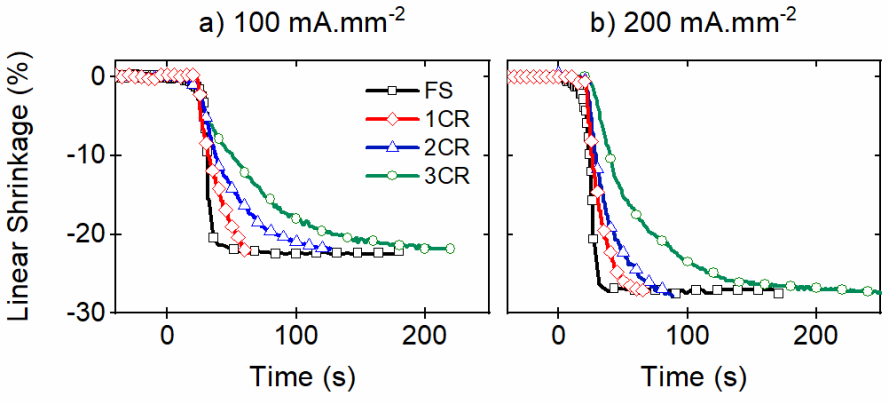

Figure 3. Linear shrinkage as a function of time for FS and CR samples treated at 100 and 200 mA·mm^{-2}.

Table 2 presents the mean values of the final linear shrinkage, apparent density, and grain size in the core and at the curved surface for all the conditions studied. For the same electric current density, there were no significant differences in the linear shrinkage. However, when all the FS and CR conditions are compared, the linear shrinkage values differ significantly. This difference can also be observed in Figure 3, in which samples treated at 200 mA·mm^{-2} show higher linear shrinkage than samples treated at 100 mA·mm^{-2}.

Table 2. Mean values of final shrinkage, apparent density, and grain size in the core and curved surface regions.

Sample	Shrinkage (%)	Apparent density (% TD)	Average grain size (μm)	
			Curved surface	Core
1FS	22.5 ± 1.3	93.9 ± 1.5	0.5 ± 0.2	1.3 ± 0.7
1CR100	22.4 ± 0.3	85.1 ± 0.8	0.3 ± 0.1	0.5 ± 0.2
2CR100	21.8 ± 0.6	92.0 ± 0.9	0.3 ± 0.1	0.5 ± 0.2
3CR100	21.8 ± 0.6	93.0 ± 1.9	0.3 ± 0.1	0.5 ± 0.2
2FS	26.9 ± 1.3	91.6 ± 1.2	0.9 ± 0.6	14.9 ± 7.5
1CR200	27.3 ± 1.9	91.4 ± 1.2	0.7 ± 0.3	11.3 ± 4.8
2CR200	28.7 ± 2.3	92.0 ± 0.9	0.8 ± 0.3	9.1 ± 6.2
3CR200	27.3 ± 1.3	92.3 ± 1.4	0.7 ± 0.3	8.2 ± 3.4

Francis and Raj[31] suggested that the superplasticity of 3YSZ during FS under mechanical pressure produces higher values of the uniaxial deformation (higher linear shrinkage) than those obtained under conventional sintering (without an electric field). Therefore, the higher shrinkage values observed in samples treated at 200 $mA{\cdot}mm^{-2}$ may be related to the superplasticity that 3YSZ exhibits during FS. The superplasticity is proportional to the temperature of the material.[32] Higher electric current densities result in higher temperatures.[33] Thus, the material is expected to exhibit superplasticity at the applied electric current density.

Table 2 shows that the apparent densities of samples 3CR100 and 3CR200 are very similar to those of samples 1FS and 2FS, respectively. This indicates that there is a direct relationship between the energy supplied by the PS and the sample densification. The apparent density of the samples increased with increasing duration of the electric current

ramp. Thus, samples with more time under the effect of the electric current had a higher apparent density. Similar results were reported in the literature.[15,16] However, the apparent densities obtained under all the conditions were similar, with the exception of the 1CR100 sample. This sample was submitted to a higher electric current ramp rate (1.64 $mA \cdot mm^{-2} \cdot s^{-1}$), and consequently to a lower energy density (23.08 $J \cdot mm^{-3}$), resulting in less densification.

Figure 4 presents SEM micrographs of the core and curved surface regions of samples 1FS, 2FS, 3CR100, and 3CR200. The images of samples 2FS and 3CR200 show that the grains in the cores of these samples [Figure 4 (a) and 4 (c)] are much larger than those on the curved surfaces [Figure 4 (b) and 4 (d)]. In addition, porosity was observed in the core region, as shown in the microstructures of the fracture surface in the core regions of samples 2FS and 3CR200 [insets in Figure 4 (a) and 4 (c), respectively]. These pores may explain why the apparent density of the samples treated at 200 $mA \cdot mm^{-2}$ is the same as that of the samples sintered at 100 $mA \cdot mm^{-2}$, although it was expected to be higher, as suggested by Francis et al.[7]

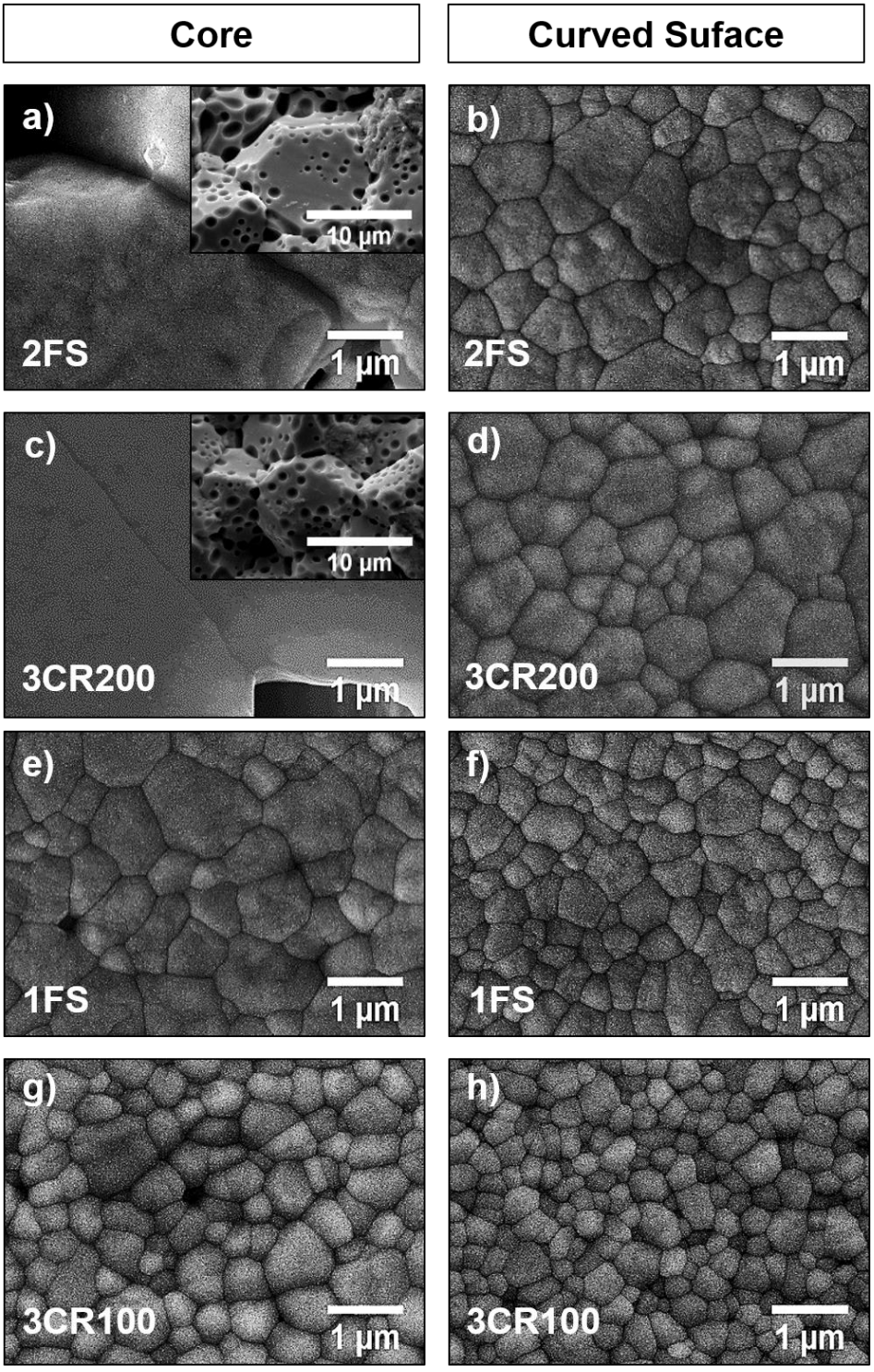

Figure 4. Microstructure of the core region of samples a) 2FS, c) 3CR200, e) 1FS, and g) 3CR100 and the curved surface region of samples b) 2FS, d) 3CR200, f) 1FS, and h) 3CR100. The insets show the core

microstructure of fractured samples, where the characteristic cavitation pores are observed.

Note that the pores observed in the insets in Figure 4 (a) and 4 (c) are not residual sintering pores. These pores appear in the presence of large grains, a phenomenon that was also observed by Baraki et al.[6] and Dong and Chen[34] in flash-sintered cylindrical 8YSZ samples. The presence of the pores can be explained by cavitation at grain boundaries, as shown in the microstructure of the fracture surfaces in the insets of Figure 4 (a) and 4 (c). Cavitation can be observed mainly in grains that have grown considerably from the particle size of the initial powder.[34]

Dong and Chen[34] suggested that cavitation can be due to reduction-generated voids by condensation of supersaturated oxygen vacancies. This condensation is accompanied by reorganization of lattice cations, which are pushed into the cavity surfaces, forming voids. According to Dong and Chen[34], when no atmospheric control is used, this cavitation occurs only in the region of the sample near the cathode, where the pores also originate.

An AC electric field was used in the FS and CR experiments, so the poles (cathode and anode) alternated during sintering. Thus, more cavitation could occur in the core region of the 2FS and 3CR200 samples, making this region porous. Blackening was not verified on samples after furnace cooling down. Although samples could have been re-oxidized during the cooling process as it happened in an oxidizing atmosphere. In addition, the alternation of the poles during sintering favors a homogeneous temperature distribution in regions of the sample in direct contact with the electrodes. This is not observed in experiments using DC electric fields, where the cathode has a lower temperature than the anode when no platinum paste is used, as demonstrated by Biesuz et al.[20]

Thus, a temperature gradient can occur between the surface and the core of the sample[15], as the temperature is much higher in the central region than at the surface. Consequently, more grain growth occurs in the core than at the sample surface owing to the higher temperature, increasing the number of cavitation pores.

Steil et al.[12] observed higher densities in cylindrical samples of 8YSZ flash-sintered at 200 $mA \cdot mm^{-2}$. However, as the holding time of the PS under this electric current was increased, the densification decreased. Thus, the magnitude of the electric current density and the holding time are important parameters that influence the densification and microstructure of the sintered material.[12,35]

In this work, differences in microstructure were observed between the core and curved surface regions of samples sintered by flash sintering. This heterogeneity was also observed in samples sintered using a CR under an electric current density of 200 $mA \cdot mm^{-2}$. In addition, this heterogeneity was much greater in the flash-sintered samples treated at 200 $mA \cdot mm^{-2}$ than in those treated at 100 $mA \cdot mm^{-2}$, as shown in Table 2.

The heterogeneity observed in the microstructure of different regions can be explained by the cylindrical shape of the sample. Park and Chen[36] suggested that cylindrical samples usually have a smaller surface-area-to-volume ratio than dog-bone-shaped samples. Samples with a lower surface-area-to-volume ratio retain more thermal energy in the core region than at the surface owing to heat loss by radiation.[36] During FS experiments, the sample heats very rapidly, almost instantaneously, which favors the formation of a temperature gradient between the core and surface of cylindrical samples. Thus, because grain growth is proportional to the temperature, the grain size heterogeneity in the microstructure of these samples can be attributed to this phenomenon.

Kumar et al.[15] sintered dog-bone-shaped 3YSZ samples using CRs with different ramp rates in an isothermal experiment (in which a PS was switched on only when a predetermined temperature was reached). They observed that a lower electric current ramp rate results in lower sample heating rates. A CR with slower ramp rates limited the Joule heating, avoiding or at least controlling thermal runaway. In this way, the heat was diffused homogeneously through the sample, increasing the heat flow from the core to the curved surface and reducing the grain size heterogeneity throughout the sample.

Sample 3CR100 has similar grain sizes in the core [Figure 4 (g)] and at the curved surface [Figure 4 (h)]. This behavior was also observed for the other CR samples treated at 100 $mA{\cdot}mm^{-2}$ (Table 2). Terauds et al.[37] suggested that in the steady state (after the flash event), almost all the electrical energy supplied by the PS is removed by thermal radiation through the sample surface. Consequently, the temperature of the sample during FS can be estimated from a model of blackbody radiation (BBR).[37] The model must be adjusted for samples sintered using a CR, because there is no steady state under these conditions.

Kumar et al.[15] modified the BBR model and proposed a relationship between the ramp rate of the electric current and the heating rate. They assumed that heating was due to the Joule effect and heat loss was due mainly to radiation. According to this model, the CR samples are expected to exhibit a lower heating rate than samples treated by conventional FS. Thus, in sintering using a CR, when a lower electric current ramp rate is used, the temperature should be more similar to that in conventional sintering (without an applied electric field).[15,38]

Figure 5 shows the results of a Tukey test comparing the grain sizes in the core and at the curved surface. Near-zero values of Tukey's mean

difference indicate higher microstructural homogeneity. Only samples 1CR100, 2CR100, and 3CR100 exhibited microstructural homogeneity at a significance level of 5%.

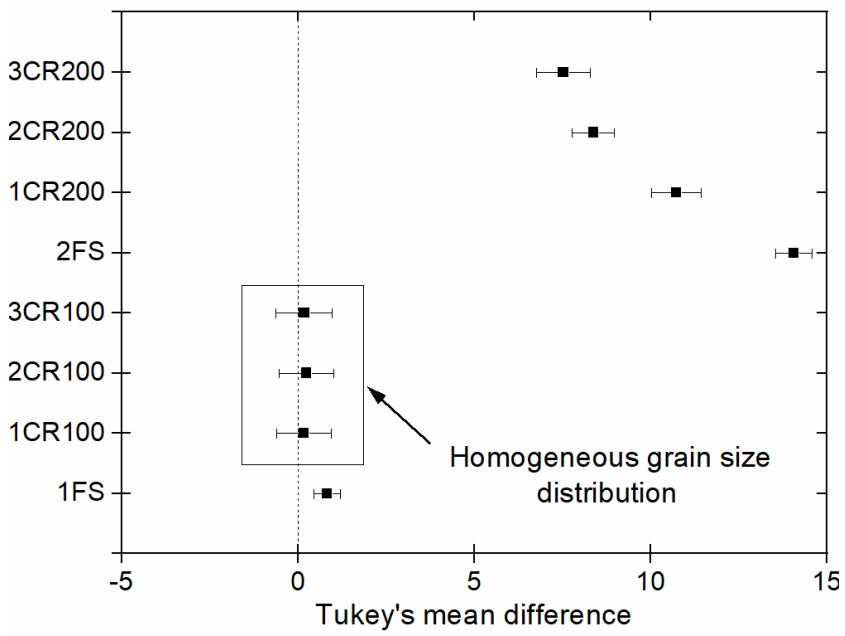

Figure 5. Tukey's mean difference between the mean grain sizes of the core and curved surface of each type of sample. Mean difference values closer to zero indicate greater microstructural homogeneity.

The CR samples treated at an electric current density of 200 mA·mm^{-2} did not show similar grain sizes in the core and at the curved surface. This result suggests that at higher maximum electric current densities, a CR with a lower ramp rate should be applied to obtain more homogeneous microstructure.

Samples treated at 200 mA·mm^{-2} generally had larger grains in each sample region (core or curved surface) than samples treated at 100 mA·mm^{-2}. The magnitude of the electric current is directly proportional to the Joule heating because the electrical resistivity of the sample at a given temperature is characteristic of the material.[7] Thus, more Joule heating,

and consequently more grain growth, occur at higher electric current density.[7,39]

Note that the microstructures of the samples treated using different CR rates had smaller grains in each region than the flash-sintered samples at the same maximum electric current density. This behavior may be related to the fact that the CR does not exhibit a peak power density, in contrast to flash sintering. According to Charalambous et al.[25], this power peak may be related to higher sample heating, with a consequent increase in grain size.

Conclusions

The electric current density was found to be a fundamental parameter affecting sample densification during flash sintering with a CR, as the linear shrinkage increased with increasing ramp rate of the CR. The use of a CR prevented both grain size heterogeneity and cavitation pores in the 3YSZ samples treated at a lower current density.

The samples sintered by FS and a CR at a higher electric current density exhibited grain size heterogeneity between the core and curved surface. In addition, cavitation pores were observed in the sample core.

At a lower electric current density, the CR was more efficient than FS in densifying 3YSZ and obtaining a homogeneous grain size in the core and curved surface regions.

Acknowledgements

Funding: This work was supported by the São Paulo State Research Support Foundation (FAPESP) [2015/07319-8, and 2018/04331-5], and the Coordination for the Improvement of Higher Education Personnel - Brazil (CAPES) [001].

References

1. Cologna M, Rashkova B, Raj R. Flash sintering of nanograin zirconia in < 5 s at 850°C. J Am Ceram Soc.2010;93(11):3556–9. doi:10.1111/j.1551-2916.2010.04089.

2. Prette AL, Cologna M, Sglavo V, Raj R. Flash-sintering of Co_2MnO_4 spinel for solid oxide fuel cell applications. J Power Sources.2011;196(4):2061–5. doi:10.1016/j.jpowsour.2010.10.036.

3. Raftery AM, Pereira da Silva JG, Byler DD, Andersson DA, Uberuaga BP, Stanek CR, et al. Onset conditions for flash sintering of UO_2. J Nucl Mater.2017;493:264–70. doi:10.1016/j.jnucmat.2017.06.022.

4. Nie J, Zhang Y, Chan JM, Huang R, Luo J. Water-assisted flash sintering: Flashing ZnO at room temperature to achieve ~ 98% density in seconds. Scr Mater.2018;142:79–82. doi:10.1016/j.scriptamat.2017.08.032.

5. Biesuz M, Sglavo VM. Flash sintering of alumina: Effect of different operating conditions on densification. J Eur Ceram Soc.2016;36(10):2535-42. doi:10.1016/j.jeurceramsoc.2016.03.021.

6. Baraki R, Schwarz S, Guillon O. Effect of electrical field/current on sintering of fully stabilized zirconia. J Am Ceram Soc.2012;95(1):75-8. doi:10.1111/j.1551-2916.2011.04980.x.

7. Francis JS, Raj R. Influence of the field and the current limit onflash sintering at isothermal furnace temperatures. J Am Ceram Soc.2013;96(9):2754–8. doi:10.1111/jace.12472.

8. Schmerbauch C, Gonzalez-Julian J, Röder R, Ronning C, Guillon O. Flash sintering of nanocrystalline zinc oxide and its influence on

microstructure and defect formation. J Am Ceram Soc.2014; 97(6):1728–35. doi:10.1111/jace.12972.

9. Jesus LM, Silva RS, Raj R, M'Peko JC. Electric field-assisted flash sintering of $CaCu_3Ti_4O_{12}$: Microstructure characteristics and dielectric properties. J Alloys Compd.2016;682:753–8. doi:10.1016/j.jallcom.2016.05.002.

10. Campos JV, Lavagnini IR, de Sousa RV, Ferreira JA, Pallone EMJA, Development of an instrumented and automated flash sintering setup for enhanced process monitoring and parameter control. J Eur Ceram Soc.2019;39(2-3):531–8. doi:10.1016/j.jeurceramsoc.2018.09.002.

11. Muccillo R, Muccillo E. Electric field-assisted flash sintering oftin dioxide. J Eur Ceram Soc.2014;34(4):915–23. doi:10.1016/j.jeurceramsoc.2013.09.017.

12. Steil MC, Marinha D, Aman Y, Gomes JRC, Kleitz M. From conventional ac flash-sintering of YSZ to hyper-flash and double flash. J Eur Ceram Soc.2013;33(11):2093–101. doi:10.1016/j.jeurceramsoc.2013.03.019.

13. Carvalho S, Muccillo E, Muccillo R. Electrical behavior and microstructural features of electric field-assisted and conventionally sintered 3 mol% yttria-stabilized zirconia. Ceramics.2018;1:1–10. doi:10.3390/ceramics1010002.

14. Demirskyi D, Vasylkiv O. Hot-spots generation, exaggerated grain growth and mechanical performance of silicon carbide bulks consolidated by flash spark plasma sintering. J Alloys Compd.2017; 691:466–73. doi:10.1016/j.jallcom.2016.08.234.

15. Kumar MKP, Yadav D, Lebrun J-M, Raj R. Flash sintering with current rate: A different approach. J Am Ceram Soc.2018;00:1-13.https://doi.org/10.1111/jace.16037

16. Bichaud E, Chaix JM, Carry C, Kleitz M, Steil MC. Flash sintering incubation in Al_2O_3/TZP composites. J Eur Ceram Soc.2015;35:2587–92. doi:10.1016/j.jeurceramsoc.2015.02.033.

17. Trombin F, Raj R. Developing processing maps for implementing flash sintering into manufacture of whiteware ceramics. Am Ceram Soc Bull.2014; 93(6):32–5.

18. Dong Y. On the Hotspot Problem in Flash Sintering, Department of Materials Science and Engineering, University of Pennsylvania, Philadelphia (USA), 2017https://arxiv.org/abs/1702.05565.

19. Ren K., Xia J, Wang Y. Grain growth kinetics of 3 mol. % yttria-stabilized zirconia during flash sintering. J Eur Ceram Soc.2019;39(4):1366–73. https://doi.org/10.1016/j.jeurceramsoc.2018.11.032

20. Biesuz M, Pinter L, Saunders T, Reece M, Binner J, Sglavo VM, et al. Investigation of electrochemical, optical and thermal effects during flash sintering of 8YSZ. Materials.2018;11(7):pii:E1214.. doi:10.3390/ma11071214.

21. Janek J, Korte C. Electrochemical blackening of yttria-stabilized zirconia – morphological instability of the moving reaction front. Solid State Ionics.1999;116(3-4):181–95. doi:10.1016/S0167-2738(98)00415-9.

22. Du Y, Stevenson AJ, Vernat D, Diaz M, Marinha D. Estimating Joule heating and ionic conductivity during flash sintering of 8YSZ. J Eur Ceram Soc.2016; 36(3):749–59. doi:10.1016/j.jeurceramsoc.2015.10.037.

23. Liu G, Liu D, Liu J, Gao Y, Wang Y. Asymmetric temperature distribution during steady stage of flash sintering dense zirconia. J Eur Ceram Soc.2018;38(7):2893–6. doi:10.1016/j.jeurceramsoc.2018.02.012.

24 Phuah XL, Wang H, Charalambous H, Jha SK, Tsakalakos T, Zhang X, et al. Comparison of the grain growth behavior and defect structures of flash sintered ZnO with and without controlled current ramp. Scr Mater.2019;162:251–5. doi:10.1016/j.scriptamat.2018.11.009.

25. Charalambous H, Jha SK, Lay RT, Cabales A, Okasinski J, Tsakalakos T. Investigation of temperature approximation methods during flash sintering of ZnO, Ceram Int.2018; 44(6)6162–9. doi:10.1016/j.ceramint.2017.12.250.

26. Charalambous H, Jha SK, Christian KH, Lay RT, Tsakalakos T. Flash Sintering using Controlled Current Ramp. J Eur Ceram Soc.2018;38(10):3689–93. doi:10.1016/j.jeurceramsoc.2018.04.003.

27. Chinelatto ASA, Chinelatto AL, Ojaimi CL, Ferreira JA, Pallone EMJA. Effect of sintering curves on the microstructure of alumina-zirconia nanocomposites. Ceram Int.2014;40(9):14669–76. doi:10.1016/j.ceramint.2014.06.055.

28, ASTM International, ASTM C 373-88 - Standard Test Method for Water Absorption, Bulk Density, Apparent Porosity, and Apparent Specific Gravity of Fired Whiteware Products, West Conshohocken ASTM Int. (2006).

29. Todd RI, Zapata-Solvas E, Bonilla RS, Sneddon T, Wilshaw PR. Electrical characteristics of flash sintering: Thermal runaway of Joule heating. J Eur Ceram Soc.2015; 35(6):1865–77. doi:10.1016/j.jeurceramsoc.2014.12.022.

30. Biesuz M, Sglavo VM, Flash sintering of ceramics. J Eur Ceram Soc.2019;39(2-3):115–43. https://doi.org/10.1016/j.jeurceramsoc.2018.08.048

31. Francis JSC, Raj R. Flash-sinterforging of nanograin zirconia: Field assisted sintering and superplasticity. J Am Ceram Soc.2012; 95(1):138–46. doi:10.1111/j.1551-2916.2011.04855.x

32. Wakai F, Sakaguchi S, Matsuno Y. Superplasticity of Yttria-Stabilized Tetragonal ZrO_2 Polycrystals, Adv. Ceram. Mater.1986;1:259–63.

33. Raj R. Joule heating during flash-sintering. J Eur Ceram Soc.2012;32(10):2293–301. doi:10.1016/j.jeurceramsoc.2012.02.030.

34. Dong Y, Chen I. Electrical and hydrogen reduction enhances kinetics in doped zirconia and ceria: II. Mapping electrode polarization and vacancy condensation in YSZ. J Am Ceram Soc.2018;101:1058–73. doi:10.1111/jace.15274.

35. Liu D, Gao Y, Liu J, Wang Y, An L. Effect of holding time on the microstructure and properties of flash-sintered Y_2O_3-doped ZrO_2. Ceram Int.2016;42:17442–6. doi:10.1016/j.ceramint.2016.08.048.

36. Park J, Chen I. *In Situ* thermometry measuring temperature flashes exceeding 1,700°C in 8 mol% Y_2O_3-stablized zirconia under constant-voltage heating. J Am Ceram Soc.2013; 96(3)697–700. doi:10.1111/jace.12176.

37. Terauds K, Lebrun JM, Lee HH, Jeon TY, Lee SH, Je JH, et al. Electroluminescence and the measurement of temperature during Stage III of flash sintering experiments. J Eur Ceram Soc.2015;35(11):3195–9. doi:10.1016/j.jeurceramsoc.2015.03.040.

38. Ji W, Parker B, Falco S, Zhang JY, Fu ZY, Todd RI. Ultra-fast firing: Effect of heating rate on sintering of 3YSZ, with and without an electric field. J Eur Ceram Soc.2017;37(6)2547–51. doi:10.1016/j.jeurceramsoc.2017.01.033.